Validation of EO-1 Hyperion and Advanced Land Imager Using the Radiometric Calibration Test Site at Railroad Valley, Nevada

Jeffrey Czapla-Myers, Lawrence Ong, Kurtis Thome, and Joel McCorkel

***Abstract*—The Earth-Observing One (EO-1) satellite was launched in 2000. Radiometric calibration of Hyperion and the Advanced Land Imager (ALI) has been performed throughout the mission lifetime using various techniques that include ground-based vicarious calibration, pseudo-invariant calibration sites, and also the moon. The EO-1 mission is nearing its useful lifetime, and this work seeks to validate the radiometric calibration of Hyperion and ALI from 2013 until the satellite is decommissioned. Hyperion and ALI have been routinely collecting data at the automated Radiometric Calibration Test Site [RadCaTS/Railroad Valley (RRV)] since launch. In support of this study, the frequency of the acquisitions at RadCaTS has been significantly increased since 2013, which provides an opportunity to analyze the radiometric stability and accuracy during the final stages of the EO-1 mission. The analysis of Hyperion and ALI is performed using a suite of ground instrumentation that measures the atmosphere and surface throughout the day. The final product is an estimate of the top-of-atmosphere (TOA) spectral radiance, which is compared to Hyperion and ALI radiances. The results show that Hyperion agrees with the RadCaTS predictions to within 5% in the visible and near-infrared (VNIR) and to within 10% in the shortwave infrared (SWIR). The 2013–2014 ALI results show agreement to within 6% in the VNIR and 7.5% in the SWIR bands. A cross-comparison between ALI and the Operational Land Imager (OLI) using RadCaTS as a transfer source shows agreement of 3%–6% during the period of 2013–2014.**

***Index Terms*—Advanced Land Imager (ALI), calibration, Earth-Observing One (EO-1), Hyperion, hyperspectral, validation.**

I. Introduction

THE EO-1 satellite was launched as a mission to demonstrate new instruments and technology as part of the NASA new millennium program [1]. The platform includes Hyperion, which is a hyperspectral imaging spectrometer, and the Advanced Land Imager (ALI), which is a multispectral sensor. Hyperion and ALI served as the stepping stones for other instruments such as Operational Land Imager (OLI) on Landsat 8 and the Hyperspectral Infrared Imager (HyspIRI), both for the demonstration of improved technology and also to simulate the expected scientific results of future missions [2]–[6]. The EO-1 platform is capable of pointing in any arbitrary direction except for some orientations in which, e.g., the instruments' boresights or radiators are in direct view of the sun. Typical earth-viewing angles for EO-1 scenes are within $\pm 23^{\circ}$, which allows EO-1 to view a given location five times during every 16-day period. The pointing agility allows the onboard sensors to be used for scientific studies that benefit from a higher temporal resolution, and it also allows more data to be collected at RadCaTS than that of a typical nadir-viewing system. During the first few years of the mission, EO-1 was placed into orbit as part of the Earth-Observing System (EOS) AM constellation [7], which allowed the cross-comparison of Hyperion and ALI with sensors such as the Landsat 7 Enhanced Thematic Mapper Plus (ETM+) and the Moderate Resolution Imaging Spectroradiometer (MODIS) onboard Terra [8], [9]. During the period 2006–2007, EO-1 performed a series of orbit maneuvers that lowered it from the 705 km circular orbit of the EOS AM constellation into a 690-km orbit. Reentry maneuvers were originally set to begin in 2012, but EO-1 was allowed to use all of its fuel to maintain a 10:00 mean local time equatorial crossing. After consuming all of its fuel in 2011, EO-1 began precessing to an earlier equatorial crossing time. The decommissioning phase is anticipated to start sometime in 2016 [1].

A. Hyperion

The Hyperion instrument is the first civilian, and the only currently available, hyperspectral imaging spectroradiometer used for earth observation [10]. It is a grating-based instrument that operates in the solar-reflective regime (400–2500 nm). It has 220 contiguous spectral bands and 12-bit radiometric resolution. It has a pixel size of 30 m, which is similar to other earth-observing sensors such as the Landsat 5 Thematic Mapper (TM), Landsat 7 ETM+, and Landsat 8 OLI, and it has a relatively small swath width of 7.7 km. The sensor design is in a pushbroom configuration, which allows for an improved signal-to-noise ratio (SNR) over sensors that use a whiskbroom configuration. The Hyperion optical system consists of one telescope that directs light into two spectrometers that disperse the light onto the VNIR (400–1000 nm) and SWIR (900–2500 nm) focal planes. The absolute radiometric accuracy specification was defined to be 6% (1σ), and extensive testing was completed

Manuscript received September 14, 2014; revised July 12, 2015; accepted July 15, 2015. Date of publication September 10, 2015; date of current version February 09, 2016. This work was supported by NASA under Grant NNX11AG28G and Grant NNX14AE20G.

J. Czapla-Myers is with the College of Optical Sciences, University of Arizona, Tucson, AZ 85721-0094 USA (e-mail: jscm@optics.arizona.edu).

L. Ong is with Science Systems and Applications, Inc., NASA/GSFC, Greenbelt, MD 20771 USA (e-mail: lawrence.ong@nasa.gov).

K. Thome and J. McCorkel are with the Biospheric Sciences Laboratory, NASA GSFC, Greenbelt, MD 20771 USA (email: kurtis.thome@nasa.gov; joel.mccorkel@nasa.gov).

Color versions of one or more of the figures in this paper are available online at http://ieeexplore.ieee.org.

Digital Object Identifier 10.1109/JSTARS.2015.2463101

prior to launch to characterize the radiometric, geometric, and spectral properties of Hyperion [11]–[13].

The Hyperion onboard calibration system originally consisted of two sets of lamp pairs that operate simultaneously to illuminate both the VNIR and SWIR focal planes, and a diffuse paint on the back side of the cover that reflects the solar beam into the instrument. One set of lamps failed prior to launch, so only one set was available for postlaunch calibration. A loss of convective cooling in the filaments resulted in a 30% increase in the lamp output, and the role of the lamps in the overall calibration scheme was eliminated after six months on orbit [14]. The directional and spectral reflectance of the solar diffuser was measured in the TRW laboratory prior to launch, and the first measurements with precise spacecraft pointing occurred on February 16, 2001 [15]. However, use of the role of solar calibrations in the trending of the instrument performance was also reduced due significant changes in the diffuse paint during the first few years of the mission. A postlaunch calibration strategy was developed using lunar observations and cross comparisons with other sensors over ground calibration sites because of the malfunctions in the EO-1 onboard approach. The use of ground-based vicarious calibration is important because it provides a calibration path that is independent of any onboard calibration systems.

B. Advanced Land Imager

Intended as a pathfinder mission for future earth-observing missions, many of the ALI new technologies had been incorporated in OLI (see [1] for overview). ALI was designed to have a 15° full field of view, but only 20% of the focal plane was populated since EO-1 was designated to be a technology demonstration mission. The swath width of ALI is 37 km, as compared to the fully populated 185-km swath width of OLI. The ALI spectral bands were chosen to include those already used by ETM+, but it also includes additional bands under study for use in OLI. They include a blue band (1p, which became the coastal aerosol band in OLI), two VNIR bands that originate from one ETM+ band (4 and 4p), and an additional SWIR band (5p). The 30-m spatial resolution of ALI is the same as ETM+. The center wavelength of each ALI band is shown in Table I, where the subscript p is used to denote multispectral bands that were not used in ETM+. The radiometric resolution of ALI is 12 bits, which is a $16\times$ improvement over the 8-bit resolution of ETM+. This, in combination with a higher SNR in all bands, means that ALI is capable of detecting changes in land cover on a finer level than its predecessors [16], [17]. As with Hyperion, ALI underwent extensive preflight testing in the laboratory, which included radiometric, geometric, and spectral calibration and characterization [18]–[22]. The preflight radiometric calibration uncertainty specification was 5%, and preflight testing indicated that it was at the $\pm 3.5\%$ level [23]. The ALI onboard calibration system consists of an onboard lamp system, where the lamps are housed in a small integrating sphere that illuminates the focal plane via the fold flat mirror that is located just before the focal plane. Since the output of the sphere is introduced into the optical system after the first three mirrors, it is unable to monitor any degradation that may occur in the mirrors. The second onboard calibration system consists of a Spectralon diffuser that also uses an aperture door that provided seven levels of solar illumination until its failure in July 2002 [24]. As with Hyperion, ALI also uses lunar observations and the cross comparison with other sensors to validate the radiometric calibration.

TABLE I
SPECTRAL BANDS OF EO-1 ALI

Band	Center wavelength (nm)	Spatial resolution (m)
Pan	591.6	10
1p	441.6	30
1	484.8	
2	567.2	
3	660.0	
4	790.0	
4p	856.6	
5p	1244.4	
5	1640.1	
7	2225.7	

C. Postlaunch Radiometric Calibration

The postlaunch radiometric calibration of earth-observing sensors is important to the scientific community, many of whom rely on long-term data records to monitor global change. It is important to understand if any changes have occurred to on-orbit sensors, and it is equally important to be able to place them on an absolute radiometric scale with SI traceability. The postlaunch radiometric calibration plan for Hyperion and ALI included vicarious calibration techniques such as ground-based measurements using onsite personnel [9], [25]–[29], under flights with the Airborne Visible Infrared Imaging Spectrometer (AVIRIS) [30], lunar observations [31], and the cross-comparison with other sensors [22], [32], [33]. Early postlaunch results for Hyperion showed that the radiometric calibration had changed from the preflight values by 8% in the VNIR spectrometer and 18% in the SWIR spectrometer, so the calibration coefficients were updated in December 2001. Ground-based measurements made by the remote sensing group (RSG) at the College of Optical Sciences, University of Arizona showed that the preflight calibration of Hyperion changed after launch, most notably in the blue region of the spectrum [26]. This result is consistent with the lunar calibrations, where the change at 457 nm is approximately -4%. ALI required a similar effort over time to monitor and analyze the radiometric calibration, and verify the results from the onboard systems. Vicarious field work completed by RSG (2001–2005) has shown similar agreement between the ground-based results and ALI [34]. The results from this work also showed that ALI agreed with the vicarious calibration radiometric results of Landsat 5 TM and ETM+ to within 5%.

This paper describes our recent vicarious calibration work for Hyperion and ALI in 2013–2014. The main difference between the results presented here and those from 2001–2005 is the use of RadCaTS to perform the ground-based measurements. Our radiometric calibration and validation approach is shifting from

Fig. 1. RadCaTS is located in RRV in central Nevada (left). RRV is $\sim 15 \times 15$ km in size, and the yellow square shows the location of the 1-km^2 RadCaTS area (center). The image on the right side shows the 1×1-km area and the location of the four GVRs. The four quadrants in red (e.g., pushbroom and whiskbroom) show the path that a user walks when sampling the site with a portable spectrometer for the reflectance-based approach. The white square in the middle shows the location of the Spectralon reference panel that is used by onsite personnel.

in situ measurements using onsite personnel to the automated RadCaTS approach. The pointing agility of the EO-1 spacecraft provides a unique opportunity to capture an increased amount of scenes that are compared to the RadCaTS results. In addition, RadCaTS is used to perform the cross comparison between Hyperion and ALI, and OLI. Section II describes the RadCaTS system, including a description of the surface reflectance and atmospheric measurements. Section III describes the data that were used in the analysis of Hyperion and ALI in the 2013–2014 time frame of this work. Section IV provides the results of this study, and finally, Section V presents the conclusion of this work.

II. Radiometric Calibration Test Site (RadCaTS)

A. Background

The RadCaTS facility is a suite of instruments that are used to make *in situ* measurements of the surface and atmosphere to predict the top-of-atmosphere (TOA) spectral radiance reflected from the earth's surface at any time during clear-sky conditions. It is an extension of the measurements made by ground-based personnel using the reflectance-based approach for vicarious calibration, and it is currently in use to validate the radiometric calibration and surface reflectance products of such sensors as Landsat 8 OLI, Landsat 7 ETM+, Terra and Aqua MODIS, the Multiangle Imaging Spectroradiometer (MISR), the Advanced Spaceborne Thermal Emission and Reflectance Radiometer (ASTER), and more recently the Suomi National Polar-Orbiting Partnership (NPP) Visible Infrared Imaging Radiometer Suite (VIIRS). The concept is similar to the Lake Tahoe and Salton Sea validation sites, which are inland bodies of water that are used to validate the calibration of earth-observing sensors that operate in the midwave infrared (MWIR) ($3-5\,\mu$m) and the thermal infrared (TIR) ($7-14\,\mu$m) spectral regions [35]. RadCaTS is used to validate sensors that operate in the solar-reflective spectral region ($0.4-2.5\,\mu$m). The typical output for a given date and time is the hyperspectral TOA spectral radiance, which is band averaged to the sensor that is being validated. The RadCaTS site is 1 km^2 and it is located at RRV, which has been used for the vicarious calibration of large-footprint sensors for almost 20 years [36]. It is centered at the coordinates 38.497°, $-115.690°$ and is at an altitude of 1435 m. An image of RRV and the layout of RadCaTS is shown in Fig. 1. Studies of the 1-km^2 area were completed in 2007–2008 in order to help understand the requirements for the number and location of the ground-viewing radiometers (GVRs) that are used to make surface reflectance measurements [37], [38].

B. Surface Measurements

The RadCaTS surface reflectance measurements are made using multispectral GVRs that were designed, developed, and tested at RSG [39]. The instruments have gone through various

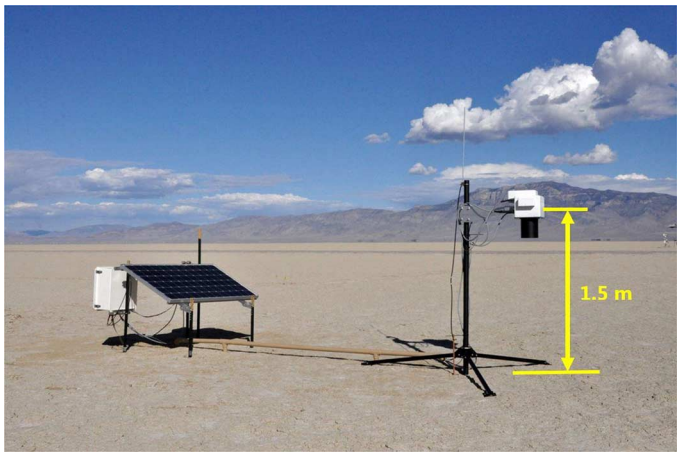

Fig. 2. GVR at RadCaTS. The white electronics box and solar panel are on the left, and the detector head is on the right. The distance from the detector plane to the ground is 1.5 m.

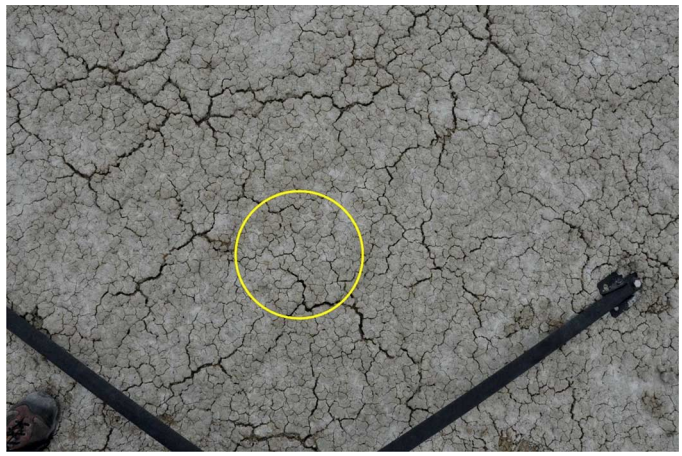

Fig. 3. Surface of RRV, as viewed from a GVR. The black objects are two of the three the tripod legs, and the yellow circle shows the 26.3-cm diameter spot on the ground that is defined by the 10° full field of view of a GVR channel.

TABLE II
SPECTRAL BANDS OF GVRS USED AT RADCATS

Band	Center wavelength (nm)	Bandwidth, FWHM (nm)
1	400	20
2	450	
3	500	
4	550	
5	650	
6	850	
7	1000	
8	1550	

Bands 1–7 use silicon detectors, and band 8 uses an INGAAS detector. The bandwidth is defined as the full width at half maximum (FWHM).

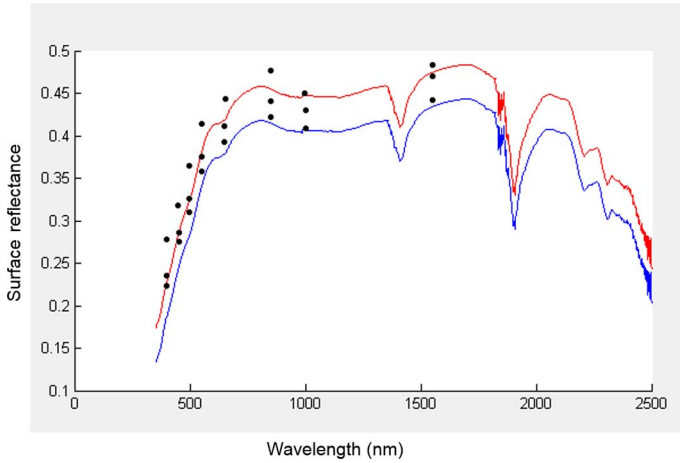

Fig. 4. RadCaTS multispectral surface reflectance, which is used to scale hyperspectral reference data for the date and time of interest. The reference data are binned into separate months, and are derived from 12 years of *in situ* measurements using ground-based personnel. The black circles represent the surface reflectance retrieved from each of three GVRs. The blue curve is the reference data that are being scaled, and the red curve is the final scaled hyperspectral reflectance for the time and date of interest.

upgrades throughout the past decade, and the current design (Fig. 2) has eight spectral channels [40]–[43]. Seven of the eight channels have silicon detectors, and the eighth channel has an InGaAs detector. Interference filters are used to control the spectral characteristics of each channel, and a summary of the center wavelength and bandwidth of each channel is shown in Table II. The full field of view of each channel is 10° (full width half maximum), and it is controlled using simple apertures [44]. The 10° field of view was chosen to ensure that the SNR is high enough without making the field of view too large. The detector plane is designed so that each channel has a slight inward tilt so that they all view the same area when the detector plane in the instrument head is placed at a height of 1.5 m. An example of the field of view is shown in Fig. 3, where the yellow line shows the approximate 26.3-cm diameter spot of each channel.

The critical electronics and focal plane of the radiometer are controlled by a thermoelectric cooler that is held at a constant 25 °C while the instrument is operating. The instruments are turned ON when the 850-nm channel output voltage is greater than a threshold value, which indicates that there is direct solar illumination on the test site surface. The instruments turn OFF when it is night, and also when there is heavy cloud cover. Each radiometer is powered by a 12-V dc battery that is charged using a solar panel. The instruments are automatically turned OFF to save battery power when the solar panels are not producing enough power to charge the system. The output voltage for each channel is digitized using an 18-bit data logger.

C. Atmospheric Measurements

Atmospheric measurements are made using a Cimel 318A sun photometer that is part of the Aerosol Robotic Network (AERONET) [45], [46]. RSG currently operates Cimel serial numbers 15 and 314. One is typically in operation at RRV while the other is being calibrated at NASA Goddard Space Flight Center (GSFC). Measurements of direct sun and sky are made throughout the day in a predetermined sequence, and the data are uploaded to GSFC via a geostationary operational environmental satellite (GOES west) every hour. The data are processed at GSFC and are downloaded by RSG for use in the RadCaTS processing code. The AERONET-derived

atmospheric properties that are required for use in the radiative transfer code are the aerosol optical depth (AOD), the Angstrom parameter, and the columnar water vapor amount. This work assumes that the spectral variation of the aerosols follows a power law, and can be defined by the AOD and the Angstrom parameter. Columnar ozone is another input required for MODTRAN, and RadCaTS uses values derived from the Ozone Monitoring Instrument (OMI), which is onboard the EOS Aura spacecraft [47]. Air temperature and pressure are also required in MODTRAN, and they are measured at RadCaTS using a meteorological station that remains onsite. It contains a Setra Model 278 barometer (Setra Systems, Boxborough, Massachusetts, USA), a Vaisala HMP35C temperature and relative humidity sensor (Vaisala Inc., Boulder, Colorado, USA), a Texas Electronics TE525WS tipping bucket rain gauge (Dallas, Texas, USA), and an R. M. Young 05103 wind monitor (Traverse City, Michigan, USA). This work uses the Chance–Kurucz exoatmospheric solar irradiance model that is contained in the MODTRAN 5 software package [48]. It has been used by RSG for Landsat 8 OLI, Landsat 7 ETM+, Landsat 5 TM, and has been used previously for the validation of Hyperion and ALI [28], [34], [49].

D. RadCaTS Data Processing

The Cimel sun photometer collects atmospheric data using its typical schedule, and the GVRs collect surface reflectance data every 2–3 min. For a given GVR, the output voltage of each channel is converted to a band-averaged spectral radiance by using the radiometric calibration coefficient determined in the laboratory prior to deployment [39], [43]. Band-averaged global spectral irradiance is determined for each of the channels by using the AERONET data as input into the MODTRAN radiative transfer code (currently version 5.3). Once the global irradiance incident on the site and the radiance reflected from the site are determined, the surface reflectance at each of the GVR's eight channels is determined for the three GVRs used in this work. It should be noted that the term "surface reflectance" is being used as a general term in this paper. RadCaTS is actually measuring the hemispherical-conical reflectance factor (HCRF), since the test site surface is illuminated from an entire hemisphere by both diffuse and direct solar components, and each GVR is measuring the reflected radiance using a finite field of view [44]. Once the surface reflectance is determined for each of the three GVRs, an average reflectance is computed at each of the eight channels. This average value is effectively the average reflectance for the 1-km^2 site at each of the eight channels.

The RadCaTS processing software requires a hyperspectral surface reflectance, so the average value determined for a given time and date at each of the GVR spectral channels is used to scale reference hyperspectral data that were obtained using a portable spectroradiometer by ground personnel who were making measurements for the reflectance-based approach. RSG has been making *in situ* surface reflectance measurements at RRV for 20 years, and the result is ~ 80 hyperspectral data sets that serve as the hyperspectral reference data for RadCaTS. The weighting of each GVR band is equal in the determination of the multispectral surface reflectance. An example of the GVR measurements being used to scale reference hyperspectral data is shown in Fig. 4. It should be noted that the fitting routine only moves the hyperspectral reference data up and down. There is no change in the spectral shape of the reference data since it is assumed that the large data set has captured the spectral features of RRV during various surface conditions throughout the year. Analysis of RadCaTS for work with Landsat 8, OLI shows that the expected uncertainty in TOA spectral radiance is 3%–4% in the wavelength range of OLI (450–2200 nm) [50]. Work is underway to analyze the uncertainty in the 400–450 and 2200–2500-nm regions.

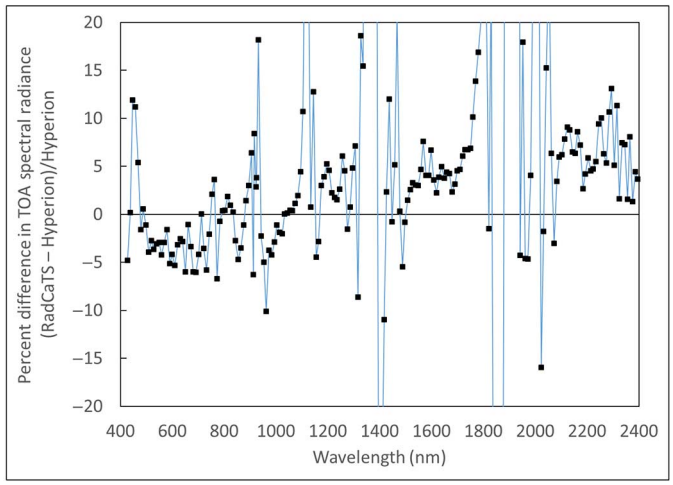

Fig. 5. Summary of the RadCaTS results for Hyperion. The results are shown as the percent difference in TOA spectral reflectance between Hyperion and RadCaTS.

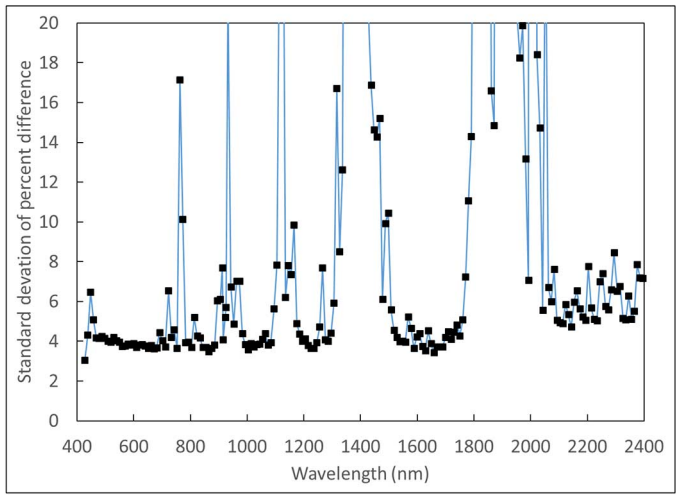

Fig. 6. 1σ standard deviation as a function of wavelength for the Hyperion results shown in Fig. 5. The large differences occur in regions that are affected by strong atmospheric absorption.

III. Data

The intensified collection of imagery of RRV by Hyperion and ALI began in early 2013, and the pointing ability of EO-1 means that more data are available than from a typical

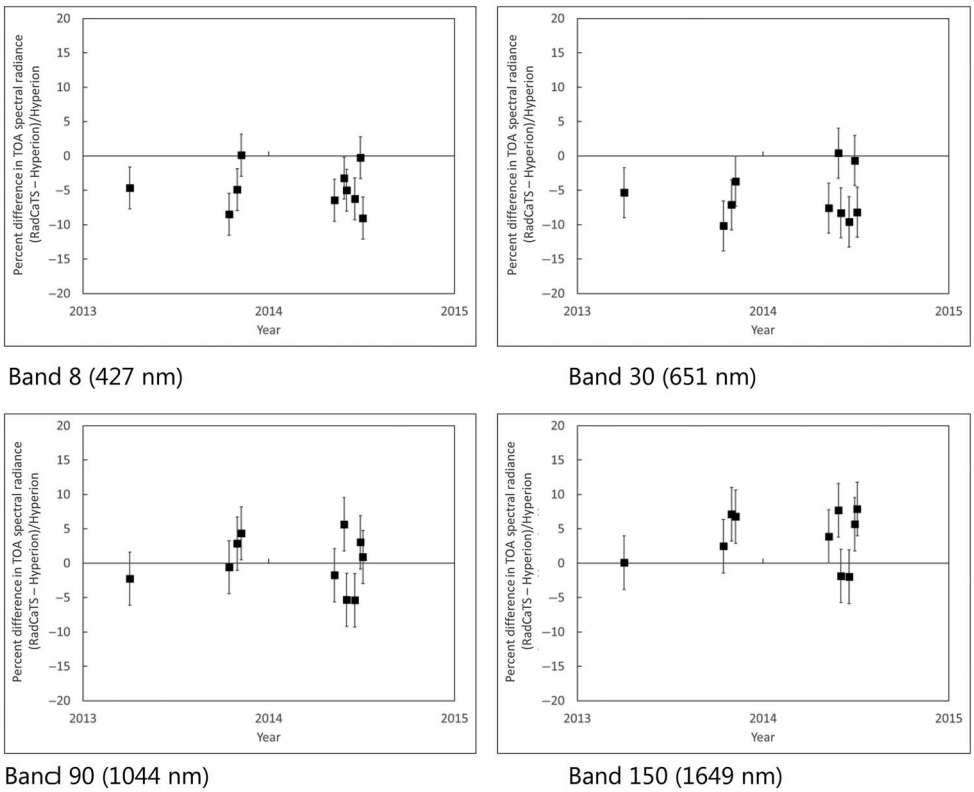

Fig. 7. Percent difference between Hyperion bands 8 (427 nm), 30 (651 nm), 90 (1044 nm), and 150 (1649 nm), and RadCaTS as a function of time.

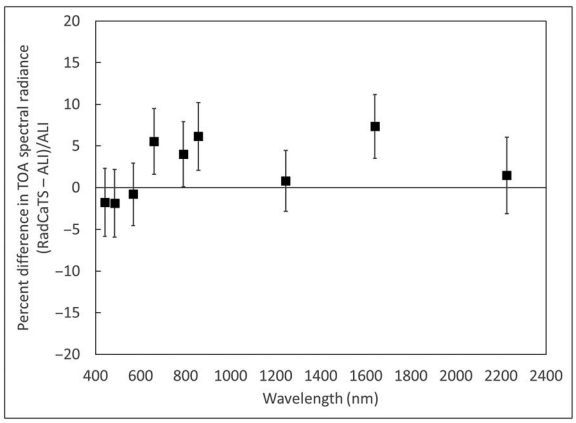

Fig. 8. Summary of the RadCaTS results for ALI. The results are shown as the percent difference in TOA spectral reflectance between ALI and RadCaTS. The uncertainty bars are the standard deviation (1σ) of the measurements.

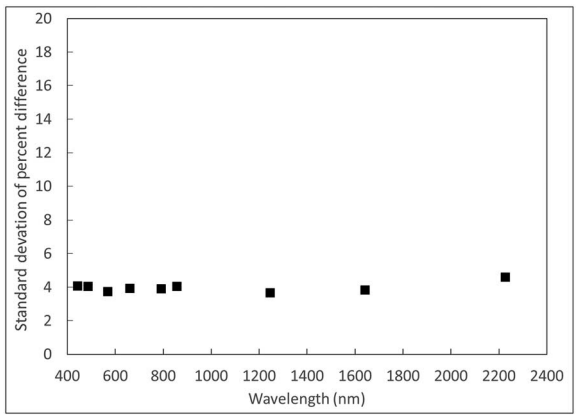

Fig. 9. 1σ standard deviation as a function of wavelength for the ALI results shown in Fig. 8.

nadir-pointing platform. During the 16-month period of this work (March 2013 to July 2014), Hyperion and ALI collected 40 images each. Of these, 10 were considered successful collections that were compared to the RadCaTS ground-based results. Typical reasons for an overpass being considered unsuccessful are clouds over the site, and water or snow on the surface. Another phenomenon that occurs after the site has dried out from a notable precipitation event is the formation of efflorescent salts on the surface. This can lead to spatial nonuniformity conditions where the areas sampled by the GVRs (26.3 cm diameter) are not indicative of the overall site, which leads to an increased uncertainty in the surface reflectance retrieval.

IV. Results

The results for Hyperion are shown in Fig. 5, which is a summary of 10 successful collections at the RadCaTS facility at RRV. The results are shown as the percent difference in the TOA spectral radiance determined by RadCaTS as compared to Hyperion. In this case, Hyperion is considered to be the correct answer, so the percent difference is given by

$$\text{Percent difference} = (\text{RadCaTS} - \text{Hyperion})/\text{Hyperion}.$$

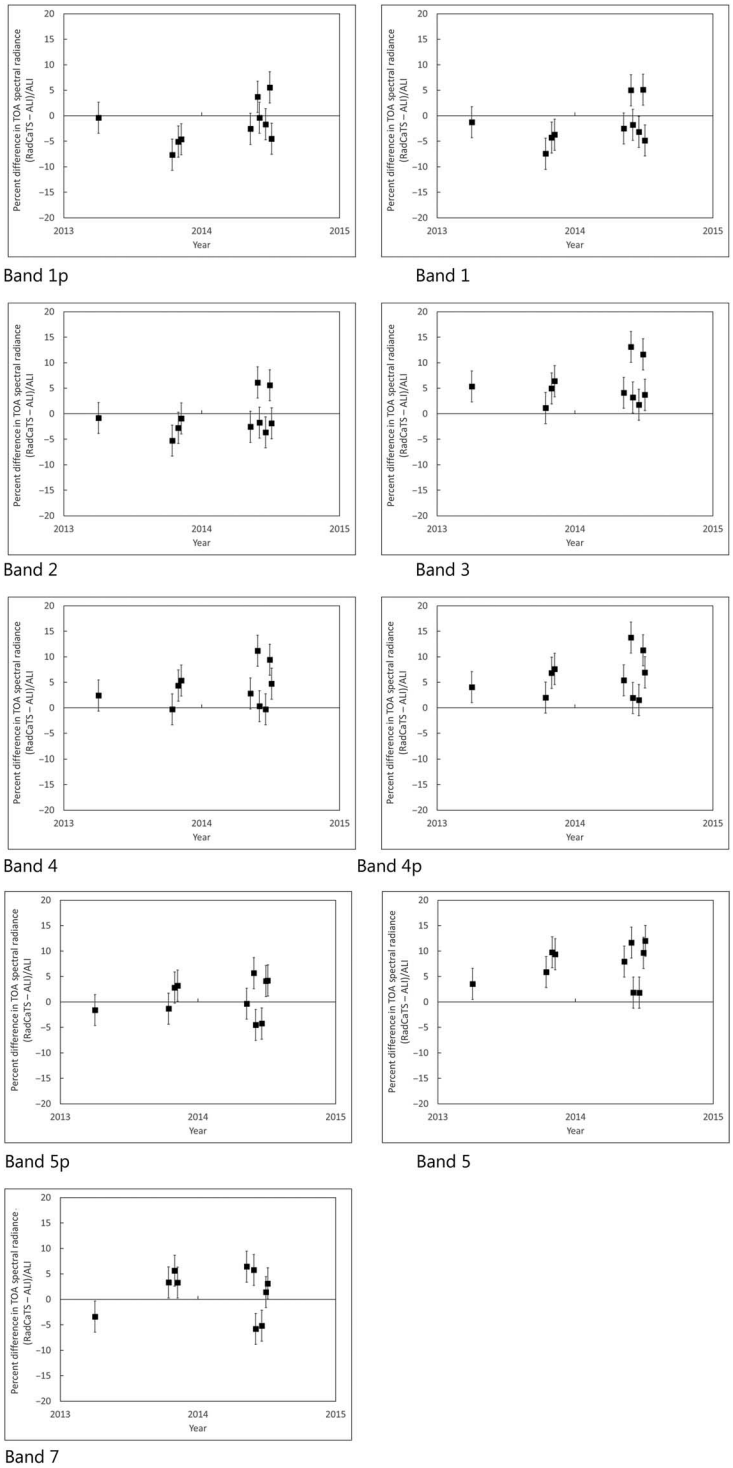

Fig. 10. Percent difference in TOA spectral radiance between ALI and RadCaTS as a function of time.

The overall shape of the percent difference as a function of wavelength is similar to the reflectance-based results from 2001–2005, but there is a slight increase in the magnitude of the values in the SWIR region. Spectral regions that contain large amounts of water vapor are generally very noisy and there is a large discrepancy between the Hyperion and RadCaTS results. The results in these regions should generally be ignored. An indication of the precision in the Hyperion results is shown in Fig. 6, where the standard deviation (1σ) of the 10 data sets is shown in Fig. 5. Throughout much of the VNIR, the standard deviation is on the order of 4%. There is a larger standard deviation in the far SWIR region (2200–2300 nm), which is 4%–7%. This is most likely due to the effects of scaling a hyperspectral reference data set in the RadCaTS processing scheme. The longest wavelength of the GVRs is 1550 nm, so there is no input in the scaling above this wavelength, which leads to higher uncertainty. In terms of trending, Fig. 7 shows the temporal results of Hyperion bands 8 (427 nm), 30 (651 nm), 90

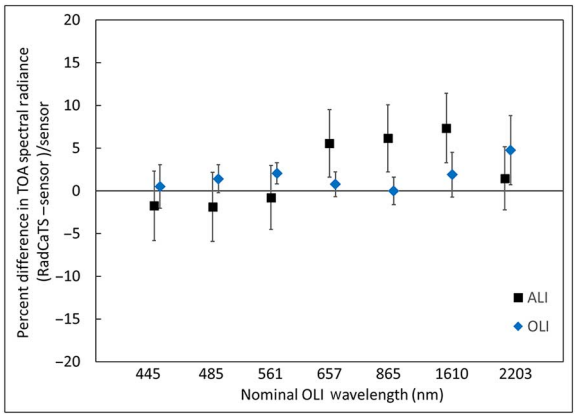

Fig. 11. Comparison between the RadCaTS results for ALI and OLI for a similar time period (2013–2014).

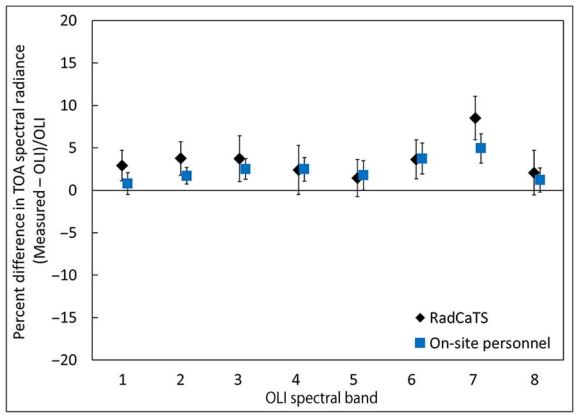

Fig. 12. Comparison between the radiometric calibration results obtained for OLI using RadCaTS and the reflectance-based approach (onsite personnel) from launch until December 2014. The uncertainty bars are the 1σ standard deviation of the measurements. Bands 1–7 are the multispectral bands, and band 8 is the panchromatic band. Band 9 (Cirrus) is not included in this work due to the extremely low SNR of the ground data.

(1044 nm), and 150 (1649 nm). In each of these cases, there does not appear to be a pattern of change. Future Hyperion collects over RRV will increase the confidence in trending analysis.

A summary of the ALI collection results for the same period as Hyperion is shown in Fig. 8, where the percent difference in TOA spectral radiance is given by

$$\text{Percent difference} = (\text{RadCaTS} - \text{ALI})/\text{ALI}.$$

The uncertainty bars are the standard deviation (1σ) of the 10 successful collects, and in the same manner as the Hyperion case, the standard deviation is also shown in Fig. 9 as a function of wavelength. Once again, the measurement precision is at the 4%–5% level. Similar to Hyperion, this phenomenon is most likely due to the uncertainty introduced by the scaling of the hyperspectral reference data in the RadCaTS processing scheme. The temporal trend of the ALI results is shown in Fig. 10, where there is no discernable pattern of degradation in the period of this study. In general, the shorter VNIR bands (1p, 1, and 2) agree to within the uncertainty of ALI and RadCaTS, but there appears to be a bias in the next three bands (3, 4, and 4p). Bands 5p and 7 agree with the RadCaTS results to within the uncertainties of the instrument and RadCaTS, but band 5 has a similar bias to RadCaTS as bands 3, 4, and 4p.

The RadCaTS results in bands 1 and 2 are similar to those from prior RSG results from 2001 to 2005, when bands 1–4 and 7 (not including the p bands) agreed with the *in situ* measurements to within $\pm 5\%$. The 2001–2005 results showed a larger bias in band 5 of 6.5%, and this is also observed in the current RadCaTS results (it should be noted that the definition of percent difference in the 2001–2005 results is reversed from the results presented here).

RadCaTS has been used to monitor OLI since the launch of Landsat 8 in February 2013, which provides the opportunity to cross-compare the validation of OLI and ALI. There have been a total of seven successful OLI collections at RadCaTS in the period from launch to July 2014. The results for OLI and the corresponding ALI bands are shown in Fig. 11, where the uncertainty bars (1σ) are the standard deviation of the measurements. There is good agreement in the coastal aerosol, blue, and breen bands, but ALI appears to have a bias of 2.5%–6.0% in the red and longer bands.

In order to evaluate the RadCaTS results for Hyperion and ALI, it is essential to compare them with results obtained using the traditional reflectance-based approach, which is still RSG's benchmark for *in situ* measurements. RSG has been validating the calibration of OLI using the reflectance-based approach and RadCaTS since launch. A summary of the current results is shown in Fig. 12, where the TOA spectral radiance reported by OLI is compared to those obtained using RadCaTS and the reflectance-based approach. The agreement between the two methods is within $\sim 2\%$ in bands 1 and 2 (coastal aerosol and blue), and $<1\%$ in bands 3–6 (green, red, NIR, and SWIR 1). There is a 3.5% bias in band 7 (SWIR 2), and this is most likely due to a combination of factors. There are no GVR bands above 1550 nm, which means that spectral bands above that wavelength do not bear any weight in the final scaling of the hyperspectral reference data.

The MODIS instruments onboard the Terra and Aqua platforms are examples of well-calibrated instruments that use a variety of techniques to validate the absolute radiometric calibration. RSG has routinely performed *in situ* measurements for both MODIS instruments since their respective launches in 1999 and 2002. A comparison between *in situ* measurements made by RSG personnel and RadCaTS is shown in Fig. 13 for MODIS land bands (1–7), and a summary is shown in Table III. The results are obtained using MODIS Collection 6 data. The Terra MODIS results from both techniques agree to within 1%, except for the blue band at 466 nm, which has a bias of $\sim 2\%$. In the Aqua MODIS case, the results between the two techniques show a larger bias of $\sim 2.5\%$ to 3.0% in the 466-, 554-, and 646-nm bands. The bias decreases to $\sim 0.5\%$ to 1.5% in the NIR and SWIR bands.

V. Discussion and Conclusion

The Radiometric Calibration Test Site (RadCaTS) at RRV has been used to validate 40 EO-1 Hyperion and ALI

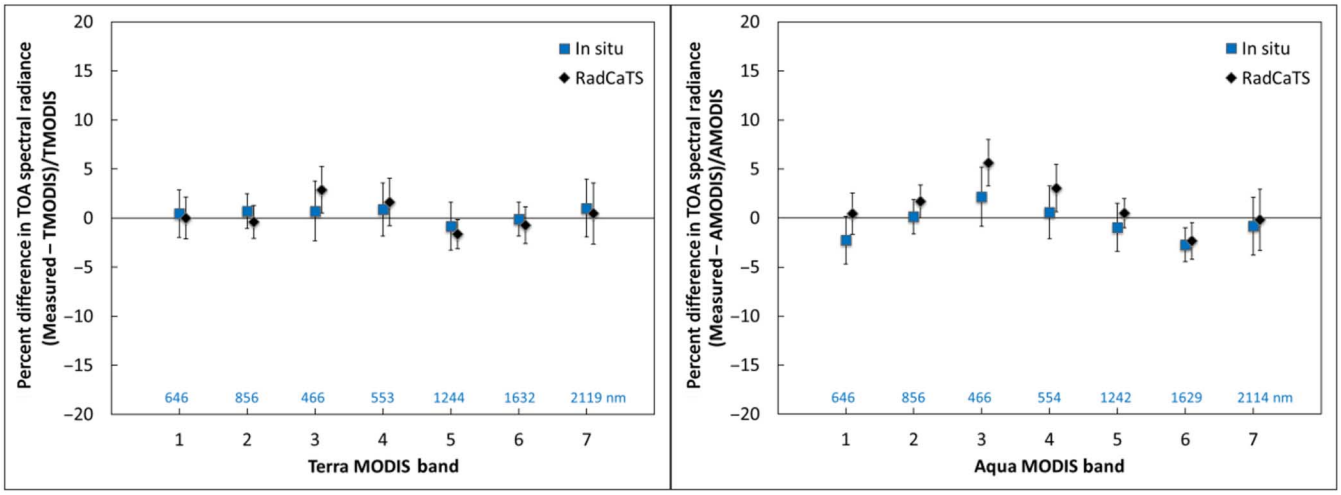

Fig. 13. Traditional reflectance-based approach (*in situ*) and RadCaTS results for Terra and Aqua MODIS.

TABLE III
SUMMARY OF THE MODIS DATA COLLECTIONS BY RSG GROUND-BASED PERSONNEL (*IN SITU*) AND RADCATS FOR THE RESULTS SHOWN IN FIG. 13

	Terra MODIS		Aqua MODIS	
	In situ	RadCaTS	*In situ*	RadCaTS
Number of data sets	21	45	14	28
Range of dates	Mar. 2000–Sep. 2014	Mar. 2012–Oct. 2014	Jul. 2002–Jun. 2011	Jan. 2012–Aug. 2014

All Terra and AQUA MODIS *in situ* data were collected at RRV using the same 1-km^2 area as RadCats.

overpasses during the period of March 2013–July 2014. This work also supplements the radiometric validation work that was performed by earlier researchers. The comparison between RadCaTS and Hyperion shows agreement to within $\pm 6\%$ at wavelengths less than 2000 nm that are not affected by atmospheric absorption. At wavelengths greater than 2000 nm, there is a 2%–10% bias between the RadCaTS and Hyperion results. There are no GVR channels at wavelengths greater than 1550 nm, so the bias in this region is mainly due to a combination of the scaling uncertainty with the hyperspectral reference curve, and the low solar irradiance in this spectral region. The ALI results show good agreement with RadCaTS in the bands below 650 nm, but there is a 4%–7% bias in the bands above 650 nm. RadCaTS results for OLI during a similar range of dates show agreement to 2% in bands 1–6 of OLI, while band 7 is in agreement with RadCaTS to within 5%. OLI has undergone extensive validation of its radiometric calibration, so the results presented here suggest that a true bias exists between OLI and ALI in bands 4–6 of OLI. Currently, there are plans to have Hyperion and ALI collect data at RRV and RadCaTS until the end of the EO-1 mission lifetime. These data will be used to analyze and validate the radiometric calibration of both instruments. In addition, the frequent acquisition of Hyperion and ALI imagery will assist RSG in analyzing the uncertainties in the RadCaTS methodology.

The larger bias between the *in situ* measurements and RadCaTS in the Aqua MODIS case may be due to the fact that a majority of the hyperspectral surface reflectance data were collected for Landsat 7 and Terra overpasses, which occur before solar noon. There may be a slight bidirectional reflectance distribution factor (BRDF) effect at RRV for measurements taken before noon, as opposed to after noon. It should be noted that the *in situ* and RadCaTS results agree to within the uncertainties of the methods.

The results of this study indicate that the RadCaTS is a valuable tool for the validation of earth-observing sensors. The original goal of RadCaTS was to collect data in the absence of ground-based personnel while retaining the same level of accuracy and precision as the reflectance-based approach. Current results show that the uncertainty in RadCaTS is higher than those obtained using the traditional reflectance-based approach. The determination of "good" and "bad" days for a given overpass at RadCaTS is currently being assessed on a case-by-case basis. It involves viewing the output voltage pattern of the GVRs over a given day, assessment of the AERONET AOD and Angstrom parameter, and cloud mask data products from MODIS and OLI. Future work is currently underway to refine the quality control process in order to determine if a given overpass should be processed or rejected.

RRV is a well-understood test site, and it has been calibrated in the spectral, spatial, and temporal domains for 20 years. The historical understanding of RRV benefits the work described here, but it should be noted that there are limitations to using one test site. For example, platforms such as Landsat, Terra, and Aqua have a nadir-view revisit time of 16 days, which means that only $\sim$23 collects with a nadir view can be made throughout the year. Wide-swath sensors such as MODIS and VIIRS are able to view the test site more often, but at larger view angles. Currently, RadCaTS is being used with sensor view angles $<15^\circ$ to minimize BRDF effects. The Working Group on Calibration and Validation (WGCV) within the Committee on Earth-Observation Satellites (CEOS) has organized an international collaboration called the Radiometric Calibration Network (RadCalNet). The goal of this working

group is to coordinate the efforts of various space agencies and research groups to facilitate the harmonization and interoperability of satellite imaging sensors with SI traceability. Currently, RadCaTS is one of the three sites used in RadCalNet. The second site is La Crau, in France, and the third is Baotou, in China. The creation of a global network of automated radiometric calibration sites will greatly increase the frequency at which data can be collected for a given sensor, especially those that have longer repeat cycles.

ACKNOWLEDGMENT

The authors would like to thank the Bureau of Land Management (BLM) Tonopah, Nevada, office for their assistance and permission in using Railroad Valley. They would also like to thank the reviewers of this paper for their comments and suggestions.

REFERENCES

[1] E. M. Middleton *et al.*, "The earth observing one (EO-1) satellite mission: Over a decade in space," *IEEE J. Sel. Topics Appl. Earth Observ. Remote Sens.*, vol. 6, no. 2, pp. 243–256, Apr. 2013.

[2] E. M. Middleton *et al.*, "Using EO-1 Hyperion images to prototype environmental products for HyspIRI," in *Proc. IEEE Int. Geosci. Remote Sens. Symp. (IGARSS)*, 2010, pp. 4256–4259.

[3] Z. Qingyuan, E. M. Middleton, G. Bo-Cai, and C. Yen-Ben, "Using EO-1 Hyperion to simulate HyspIRI products for a coniferous forest: The fraction of PAR absorbed by chlorophyll fAPAR and leaf water content (LWC)," *IEEE Trans. Geosci. Remote Sens.*, vol. 50, no. 5, pp. 1844–1852, May 2012.

[4] J. Nelson *et al.*, "Landsat data continuity mission (LDCM) space to ground mission data architecture," in *Proc. IEEE Aerosp. Conf.*, 2012, pp. 1–13.

[5] M. Abrams, D. Pieri, V. Realmuto, and R. Wright, "Using EO-1 Hyperion data as HyspIRI preparatory data sets for volcanology applied to Mt Etna, Italy," *IEEE J. Sel. Topics Appl. Earth Observ. Remote Sens.*, vol. 6, no. 2, pp. 375–385, Apr. 2013.

[6] S. P. Neeck and S. M. Volz, "NASA's Earth science missions overview," in *Proc. Sens. Syst. Next Gener. Satell. XIII*, 2009, pp. 74740B–74740B-12.

[7] D. Folta, L. K. Newman, and D. Quinn, "Design and implementation of satellite formations and constellations," in *Proc. AAS/GSFC Int. Symp. Space Flight Dyn.*, Greenbelt, MD, USA, 1998, pp. 57–70.

[8] G. Chander, A. Angal, T. J. Choi, D. J. Meyer, X. J. Xiong, and P. M. Teillet, "Cross-calibration of the Terra MODIS, Landsat 7 ETM+ and EO-1 ALI sensors using near-simultaneous surface observation over the Railroad Valley Playa, Nevada, test site," in *Proc. SPIE Earth Observ. Syst. XII*, San Diego, CA, USA, 2007, pp. 66770Y-12.

[9] K. J. Thome, S. F. Biggar, and W. Wisniewski, "Cross comparison of EO-1 sensors and other Earth resources sensors to Landsat-7 ETM+ using Railroad Valley Playa," *IEEE Trans. Geosci. Remote Sens.*, vol. 41, no. 6, pp. 1180–1188, Jun. 2003.

[10] R. Buckingham and K. Staenz, "Review of current and planned civilian space hyperspectral sensors for EO," *Can. J. Remote Sens.*, vol. 34, pp. S187–S197, Jan., 2008.

[11] J. Pearlman *et al.*, "Development and operations of the EO-1 Hyperion imaging spectrometer," *Proc. SPIE*, pp. 243–253, 2000.

[12] J. Pearlman, S. Carman, C. Segal, P. J. Jarecke, P. Clancy, and W. Browne, "Overview of the Hyperion imaging spectrometer for the NASA EO-1 mission," in *Proc. Int. Geosci. Remote Sens. Symp. (IGARSS)*, 2001, pp. 3036–3038.

[13] J. S. Pearlman, P. S. Barry, C. C. Segal, J. Shepanski, D. Beiso, and S. L. Carman, "Hyperion, a space-based imaging spectrometer," *IEEE Trans. Geosc. Remote Sens.*, vol. 41, no. 6, pp. 1160–1173, Jun. 2003.

[14] J. S. Pearlman, "Hyperion validation report," The Boeing Company, Kent, WA, USA, 2003.

[15] P. J. Jarecke, K. K. Yokoyama, and P. Barry, "On-orbit solar radiometric calibration of the Hyperion instrument," in *Proc. Imag. Spectrom. VII*, San Diego, CA, USA, 2002, pp. 225–230.

[16] M. A. Wulder *et al.*, "Landsat continuity: Issues and opportunities for land cover monitoring," *Remote Sens. Environ.*, vol. 112, pp. 955–969, Mar., 2008.

[17] A. L. Neuenschwander, M. M. Crawford, and S. Ringrose, "Results from the EO-1 experiment—A comparative study of earth observing-1 advanced land imager (ALI) and Landsat ETM+ data for land cover mapping in the Okavango Delta, Botswana," *Int. J. Remote Sens.*, vol. 26, pp. 4321–4337, Nov., 2005.

[18] W. E. Bicknell, C. J. Digenis, S. E. Forman, and D. E. Lencioni, "EO-1 advanced land imager," *Proc. SPIE*, pp. 80–88, 1999.

[19] D. R. Hearn, C. J. Digenis, D. E. Lencioni, J. A. Mendenhall, J. B. Evans, and R. D. Welsh, "EO-1 advanced land imager overview and spatial performance," in *Proc. IEEE Int. Geosci. Remote Sens. Symp. (IGARSS'01)*, 2001, vol. 2, pp. 897–900.

[20] D. E. Lencioni, C. J. Digenis, W. E. Bicknell, D. R. Hearn, and J. A. Mendenhall, "Design and performance of the EO-1 advanced land imager," *Proc. SPIE*, pp. 269–280, 1999.

[21] D. R. Hearn, J. A. Mendenhall, and B. C. Willard, "Spatial calibration of the EO-1 advanced land imager," *Proc. SPIE*, pp. 97–108, 1999.

[22] J. A. Mendenhall and A. C. Parker, "Spectral calibration of the EO-1 advanced land imager," *Proc. SPIE*, pp. 109–116, 1999.

[23] J. A. Mendenhall, D. E. Lencioni, and J. B. Evans, "Earth observing-1 advanced land imager: Radiometric response calibration," Massachusetts Inst. Technol., Cambridge, MA, USA, Project Rep. EO-1-3, 2000.

[24] B. L. Markham *et al.*, "Radiometric calibration stability of the EO-1 Advanced Land Imager: 5 years on-orbit," *Proc. SPIE*, pp. 63610U–63610U-12, 2006.

[25] S. F. Biggar, K. J. Thome, J. M. Holmes, M. A. Kuester, and R. A. Schowengerdt, "In-flight radiometric and spatial calibration of EO-1 optical sensors," in *Proc. Int. Geosci. Remote Sens. Symp. (IGARSS)*, Sydney, Australia, 2001, pp. 305–307.

[26] S. F. Biggar, K. J. Thome, and W. Wisniewski, "Vicarious radiometric calibration of EO-1 sensors by reference to high-reflectance ground targets," *IEEE Trans. Geosci. Remote Sens.*, vol. 41, no. 6, pp. 1174–1179, Jun. 2003.

[27] S. F. Biggar, K. J. Thome, and W. T. Wisniewski, "In-flight radiometric calibration of the advanced land imager and Hyperion sensors on the EO-1 platform and comparisons with other earth observing sensors," *Proc. SPIE*, pp. 289–295, 2002.

[28] J. McCorkel, K. Thome, and L. Ong, "Vicarious calibration of EO-1 Hyperion," *IEEE J. Sel. Topics Appl. Earth Observ. Remote Sens.*, vol. 6, no. 2, pp. 400–407, Apr. 2013.

[29] P. Barry, P. J. Jarecke, J. Pearlman, D. Jupp, J. Lovell, and S. Campbell, "Radiometric calibration validation of the Hyperion instrument using ground truth at a site in Lake Frome, Australia," *Proc. SPIE*, pp. 242–246, 2002.

[30] R. O. Green, B. E. Pavri, and T. G. Chrien, "On-orbit radiometric and spectral calibration characteristics of EO-1 Hyperion derived with an underflight of AVIRIS and in situ measurements at Salar de Arizaro, Argentina," *IEEE Trans. Geosci. Remote Sens.*, vol. 41, no. 6, pp. 1194–1203, Jun. 2003.

[31] H. H. Kieffer, P. J. Jarecke, and J. Pearlman, "Initial lunar calibration observations by the EO-1 Hyperion imaging spectrometer," *Proc. SPIE*, pp. 247–258, 2002.

[32] G. Chander, D. J. Meyer, and D. L. Helder, "Cross calibration of the Landsat-7 ETM+ and EO-1 ALI sensor," *IEEE Trans. Geosci. Remote Sens.*, vol. 42, no. 12, pp. 2821–2831, Dec. 2004.

[33] J. A. Pedelty, J. T. Morisette, and J. A. Smith, "Comparison of Landsat-7 enhanced thematic mapper plus (ETM+) and earth observing one (EO-1) advanced land imager," *Opt. Eng.*, vol. 43, pp. 954–962, 2004.

[34] J. McCorkel, K. Thome, S. Biggar, and M. Kuester, "Radiometric calibration of advanced land imager using reflectance-based results between 2001and 2005," *Proc. SPIE*, pp. 62960G–62960G-8, 2006.

[35] S. J. Hook, R. G. Vaughan, H. Tonooka, and S. G. Schladow, "Absolute radiometric in-flight validation of mid infrared and thermal infrared data from ASTER and MODIS on the terra spacecraft using the Lake Tahoe, CA/NV, USA, automated validation site," *IEEE Trans. Geosci. Remote Sens.*, vol. 45, no. 6, pp. 1798–1807, Jun. 2007.

[36] K. P. Scott, K. J. Thome, and M. R. Brownlee, "Evaluation of the railroad valley playa for use in vicarious calibration," in *Proc. Multispectral Imag. Terr. Appl.*, Denver, CO, USA, 1996, pp. 158–166.

[37] J. S. Czapla-Myers, K. J. Thome, and J. H. Buchanan, "Implication of spatial uniformity on vicarious calibration using automated test sites," in *Proc. Earth Observ. Syst. XII*, San Diego, CA, USA, 2007, pp. 66770U-10.

[38] J. S. Czapla-Myers, K. J. Thome, B. R. Cocilovo, J. T. McCorkel, and J. H. Buchanan, "Temporal, spectral, and spatial study of the automated vicarious calibration test site at Railroad Valley, Nevada," in *Proc. Earth Observ. Syst. XIII*, San Diego, CA, USA, 2008, pp. 70810I-9.
[39] N. J. Anderson and J. S. Czapla-Myers, "Ground viewing radiometer characterization, implementation and calibration applications: A summary after two years of field deployment," in *Proc. SPIE Opt. Eng. Appl.*, 2013, pp. 88660N-88660N-10.
[40] K. J. Thome, J. S. Czapla-Myers, and S. F. Biggar, "Ground-monitor radiometer system for vicarious calibration," in *Proc. Imag. Spectrom. X*, Denver, CO, USA, 2004, pp. 223–232.
[41] J. S. Czapla-Myers, K. J. Thome, and S. F. Biggar, "Design, calibration, and characterization of a field radiometer using light-emitting diodes as detectors," *Appl. Opt.*, vol. 47, pp. 6753–6762, 2008.
[42] J. Czapla-Myers, K. Thome, and N. Leisso, "Radiometric calibration of earth-observing sensors using an automated test site at Railroad Valley, Nevada," *Can. J. Remote Sens.*, vol. 36, pp. 474–487, 2011.
[43] N. Anderson *et al.*, "Design and calibration of field deployable ground-viewing radiometers," *Appl. Opt.*, vol. 52, pp. 231–240, 2013.
[44] G. Schaepman-Strub, M. E. Schaepman, T. H. Painter, S. Dangel, and J. V. Martonchik, "Reflectance quantities in optical remote sensing—definitions and case studies," *Remote Sens. Environ.*, vol. 103, pp. 27–42, 2006.
[45] B. N. Holben *et al.*, "AERONET—A federated instrument network and data archive for aerosol characterization," *Remote Sens. Environ.*, vol. 66, pp. 1–16, 1998.
[46] O. Dubovik *et al.*, "Accuracy assessments of aerosol properties retrieved from aerosol robotic network (AERONET) Sun and sky radiance measurments," *J. Geophys. Res.*, vol. 105, pp. 9791–9806, 2000.
[47] J. P. Veefkind, J. F. de Haan, E. J. Brinksma, M. Kroon, and P. F. Levelt, "Total ozone from the ozone monitoring instrument (OMI) using the DOAS technique," *IEEE Trans. Geosci. Remote Sens.*, vol. 44, no. 5, pp. 1239–1244, May 2006.
[48] A. Berk, G. P. Anderson, and P. K. Acharya, *MODTRAN-5.3.2 User's Manual*, 2013.
[49] J. McCorkel, K. Thome, N. Leisso, N. Anderson, and J. Czapla-Myers, "Radiometric characterization of hyperspectral imagers using multispectral sensors," in *Proc. SPIE Earth Observ. Syst. XIV*, San Diego, CA, USA, 2009, pp. 745210–745211.
[50] J. Czapla-Myers *et al.*, "The ground-based absolute radiometric calibration of Landsat 8 OLI," *Remote Sens.*, vol. 7, pp. 600–626, 2015.

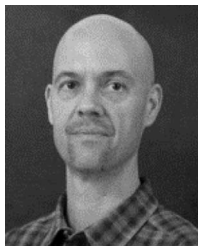

Jeffrey Czapla-Myers received the B.S. degree in optical engineering from the University of Arizona, Tucson, AZ, USA, the M.Sc. degree in earth and space science from York University, Toronto, ON, Canada, and the Ph.D. degree in optical sciences from the University of Arizona.

He is an Associate Research Professor with the College of Optical Sciences, University of Arizona. His research interests include remote sensing, radiometry, ground-based vicarious calibration of airborne and satellite systems, and the design, development, and laboratory characterization of radiometers.

Dr. Czapla-Myers is currently a member of the Landsat Calibration Working Group, a member of the MODIS Science Team, the Suomi NPP Science Team, and a Senior Member of SPIE.

Lawrence Ong received the B.S. and M.S. degrees in mechanical engineering from Oklahoma State University, Stillwater, OK, USA, and the Ph.D. degree in mechanical engineering from the University of Maryland, College Park, MD, USA.

He conducted research in turbulence processes as a research scientist at the University of Maryland before joining the MODIS Science Team, the SNPP Science Team, and Science Systems and Applications, Inc., to support remote sensing research and engineering at the EO-1 Mission Science Office at NASA's Goddard Space Flight Center (GSFC). His research interests include instrumentation, calibration/validation and applications for remote sensing and fluid dynamics.

Dr. Ong is also currently a member of the Landsat Data Continuity Mission's Calibration and Validation Team at GSFC.

Kurtis Thome received the B.S. degree in meteorology from Texas A&M University, College Station, TX, USA, and the M.S. and Ph.D. degrees in atmospheric sciences from the University of Arizona, Tucson, AZ, USA.

He was a full Professor with the College of Optical Sciences, University of Arizona, in 2006. He served as the Director of the Remote Sensing Group from 1997 to 2008. He moved to NASA's Goddard Space Flight Center in 2008 as a Physical Scientist in the Biospheric Sciences Laboratory.

Dr Thome is the Deputy Project Scientist for CLARREO for which he is also the instrument lead for the Reflected Solar Instrument. He has been a member of the Landsat 7, ASTER, MODIS, and EO-1 Science Teams providing vicarious calibration results for those and other imaging sensors. He is a Fellow of SPIE and the Instrument Scientist for the Visible Infrared Imaging Radiometer Suite (VIIRS) on the Joint Polar Satellite System, and is serving as the Lead for the Thermal Infrared Sensor on Landsat 8.

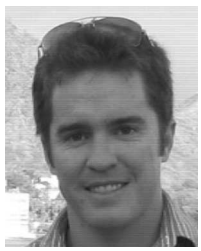

Joel McCorkel received the B.S. degree in optical engineering and the Ph.D. degree in optical sciences from the University of Arizona, Tucson, AZ, USA.

He joined the National Ecological Observatory Network as a Staff Scientist from the Airborne Observation Platform in 2009. He is currently a Physical Scientist with the Biospheric Sciences Laboratory, NASA's Goddard Space Flight Center, Greenbelt, MD, USA.